Noname manuscript No.
(will be inserted by the editor)

Multi-modality Imagery Database for Plant Phenotyping

Jeffrey A Cruz* · **Xi Yin*** · **Xiaoming Liu** · **Saif M Imran** · **Daniel D Morris** · **David M Kramer** · **Jin Chen**

Received: date / Accepted: date

Abstract Among many applications of machine vision, plant image analysis has recently begin to gain attention due to its potential impact on plant visual phenotyping, particularly in understanding plant growth, assessing the quality/performance of crop plants and improving crop yield. Despite its importance, the lack of publicly available research databases containing plant imagery has substantially hindered the advancement of plant image analysis. To alleviate this issue, this paper presents a new multi-modality plant imagery database named "MSU-PID", with two distinct properties. First, MSU-PID is captured using four types of imaging sensors, fluorescence, infrared (IR), RGB color, and depth. Second, the imaging setup and the variety of manual labels allow MSU-PID to be suitable for a diverse set of plant image analysis applications, such as leaf segmentation, leaf counting, leaf alignment, and leaf tracking. We provide detailed information on the plants, imaging sensors, calibration, labeling, and baseline performances of this new database.

Keywords Plant Phenotyping · Computer Vision · Plant image · Leaf segmentation · Leaf tracking · Multiple sensors · Arabidopsis · Bean

1 Introduction

With the rapid growth of world population and the loss of arable land, there is an increasing desire to improve the yield and quality of crops, where the understanding of the genetic mechanisms to influence plant growth is a key enabler [Döös, 2002]. A classic genetics approach is to produce a diverse population of mutant lines, grow them either in growth chambers with simulated environmental conditions or directly in the field, visually observe the plants during the growth period, and finally identify plant morphological or physiological patterns that tightly associate with key growth factors [Houle et al., 2010]. While many factors can be assessed quantitatively, which is essential for high-throughput study, one of the bottleneck in this research pipeline is plant visual phenotyping [Walter et al., 2015].

Plants develop through a complex interaction between genotype and environment. This determines their structure and functions and thus performance such as yield or efficient use of resources. In order to understand the genetic basis of these economically important parameters, it is essential to quantitatively assess plant phenotypes and then identify the latent relationships to genotypes and environmental factors. Plant visual phenotyping has been performed by farmers and breeders for more than 5,000 years. In the past, traditional phenotyping is based on experience and intuition, and is la-

* denotes equal contribution by the authors. This research was supported by Chemical Sciences, Geosciences and Biosciences Division, Office of Basic Energy Sciences, Office of Science, U.S. Department of Energy (award number DE-FG02-91ER20021), and by Center for Advanced Algal and Plant Phenotyping (CAAPP), Michigan State University.

Jeffrey A Cruz · Jin Chen · David M Kramer
Department of Energy Plant Research Laboratory, Michigan State University, East Lansing, MI 48824, USA
E-mail: {cruzj,jinchen,kramerd8}@msu.edu

Xi Yin · Xiaoming Liu (✉)
Department of Computer Science and Engineering, Michigan State University, East Lansing, MI 48824, USA
E-mail: {yinxi1,liuxm}@cse.msu.edu

Saif Imran · Daniel D Morris
Department of Electrical and Computer Engineering, Michigan State University, East Lansing, MI 48824, USA
E-mail: {imransai,dmorris}@msu.edu

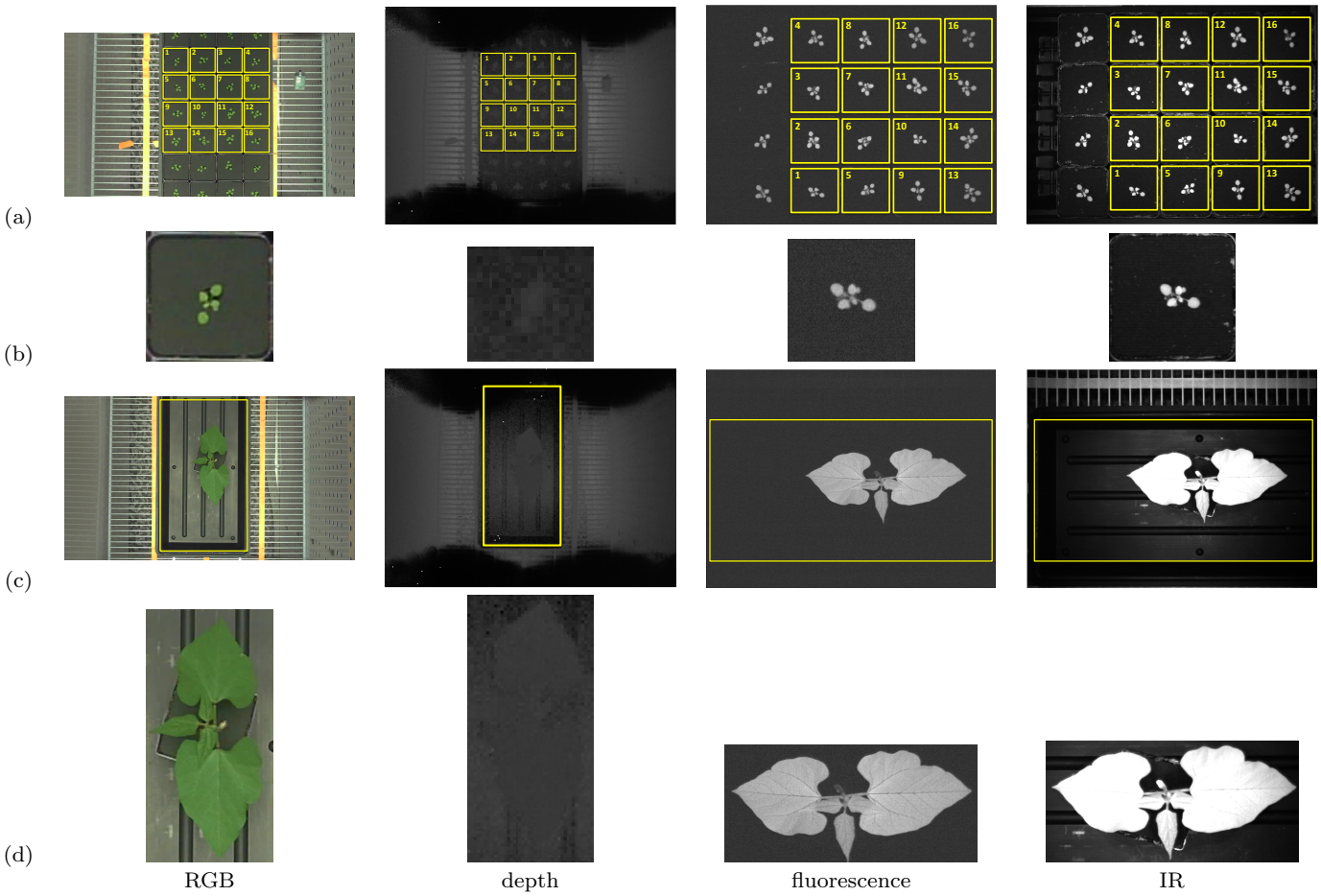

Fig. 1 The multi-modality plant imagery database of MSU-PID. (a) four modalities of Arabidopsis; (b) zoom in view of Arabidopsis plant 1; (c) four modalities of bean; (d) zoom in view of bean plant.

borious [Erblichkeit, 1903]. Recent progresses in imaging sensor, robotics and automation technologies lead to the development of the ever-increasing new field of highly automated, non-destructive *plant visual phenotyping* [Furbank & Tester, 2011, Cruz et al., 2015]. The objective of modern plant visual phenotyping is to analyze and categorize the morphological characteristics of plants, thus accurately quantifying plant traits. In this interdisciplinary field, scientists employ various imaging sensors to capture plants and design advanced algorithms to automatically analyze the captured plant imagery, with the purpose of raising testable biological hypotheses to solve problems related to growth, development, stress tolerance, resistance, and so on. A key advance in visual phenotyping is the capability to non-invasively capture plant traits, enabling continuous measurements that are necessary to monitor plants during growth and/or under stress conditions. Vision based phenotyping also increases the throughput of phenotyping experiments by eliminating destructive operations. The increased capacity allows more genotypes or biological replicates to be examined under the same environmental conditions [Fahlgren et al., 2015, Walter et al., 2015].

Due to diverse variations of leaf shape, appearance, layout, growth and movement, plant image analysis is a non-trivial computer vision task [Minervini et al., 2015]. In order to develop advanced computer vision algorithms, image databases that are well representative of this application domain is highly important. In fact, computer vision research lives on and advances with databases, as evidenced by the successful databases in the field (e.g., FERET [Phillips et al., 2000] and LFW [Huang et al., 2007]). However, the publicly available database for plant phenotyping is still very limited, with the only exception of LSC database [Scharr et al., 2014], which, nevertheless, has its own limitations on the type of images (RGB only) and is only suitable for a small set of plant image analysis applications.

Table 1 Plant image databases.

Database	Modality	Applications[a]	Plant Type	Subject/ Classe #	Total Image #	Labeled Image #
Swedish leaf [Söderkvist, 2001]	Scaned leaf	LC	Swedish trees	15	1,125	1,125
Flavia [Wu et al., 2007]	RGB	LC	Leaves	32	2,120	2,120
Leafsnap [Kumar et al., 2012]	RGB	LC	USA trees	184	29,107	29,107
Crop/weed [Haug & Ostermann, 2014]	RGB	Weed detection	Crop/weed	2	60	60
LSC [Haug & Ostermann, 2014]	RGB	LS, LO	Arabidopsis	43	6287	201
			Tobacco	80	165,120	83
MSU-PID	fluorescence, IR, RGB, depth	LS, LO, LA, LT	Arabidopsis	16	2304×4	576×4
			Bean	5	350×4	175×4

[a] The abbreviation in "Applications" column is defined as Leaf Classification (LC), Leaf Segmentation (LS), Leaf Counting (LO), Leaf Alignment (LA), and Leaf Tracking (LT).

To facilitate future research on plant image analysis, as well as remedy the limitation of existing databases in the field, this paper presents a newly collected multi-modality Plant Imagery Database through an interdisciplinary effort at Michigan State University (MSU), termed "MSU-PID". As illustrated in Figure 1, the MSU-PID database includes the imagery of two types of plants (Arabidopsis and bean), both are widely used in plant research, captured by four types of imaging sensors, i.e., fluorescence, infrared (IR), RGB color, and depth. All four sensors are synchronized and are programmed to periodically capture imagery data for multiple consecutive days. Checkerboard-based camera calibration is performed between a pair of sensors, which results in the explicit correspondence between the pixels of *any* two modalities.

The type and amount of manual labels on a database is a critical enabler to the potential applications of the database. For a subset of the MSU-PID database, we manually label the ground truth regarding the leaf identification number, locations of leaf tips and leaf segments. As a result, MSU-PID is suitable for a number of applications, including 1) *leaf segmentation* that aims at estimating the correct segmentation mask of each leaf in an image, 2) *leaf counting* that estimates the correct number of leaves within a plant, 3) *leaf alignment* that aligns the two tips of each leaf – the cornerstone of the leaf structure, and 4) *leaf tracking* that is designed to track each leaf over time. Finally, to provide a performance baseline for future research and comparison, we apply our automatic leaf segmentation framework [Yin et al., 2014a, Yin et al., 2014b] to the Arabidopsis imagery and demonstrate the unique challenge of image analysis on this database.

In summary, this paper and our database have made the following main contributions.

- MSU-PID is the first *multi-modality* plant image database. This allows researchers to study the strength and weakness of individual modality, as well as their various combinations in plant image analysis.
- Our unique imaging setup and the variety of manual labels make MSU-PID an ideal candidate for evaluating a diverse set of plant image analysis applications, including leaf segmentation, leaf counting, leaf alignment, leaf tracking, and potentially leaf growth prediction and 3D leaf reconstruction.

2 Prior Work

Databases drive computer vision research. Hence, it is always important to develop and promote properly captured databases in the vision community. While there is a clear desire to apply computer vision to plant image analysis, the lack of publicly available plant image databases has been an obstacle for the further study and development.

We summarize existing publicly available databases that are most related to our work in Table 1. In terms of potential applications of these databases, they can be categorized into two types. The first type is for the general purpose of recognizing a particular species of tree or plant. The Swedish leaf database [Söderkvist, 2001] is probably the first leaf database even though the images are captured by scanners. The Flavia database [Wu et al., 2007] is considerably larger and a neural network is utilized to train a leaf classifier. The most recent leafsnap project [Kumar et al., 2012] is an impressive effort that includes a very large dataset of leaves for 184 tree types. A mobile phone application is also developed to make the leaf classification system portable. Finally, the

crop/weed image database [Haug & Ostermann, 2014] is captured by a robot in the real field, and used for the classification of crop vs. weed. Note that except for [Haug & Ostermann, 2014] where images are captured in the wild for a large area of plant, other databases in this type normally capture only a *single* leaf is in a relatively constrained imaging environment. Therefore, the challenging problem of leaf segmentation has been bypassed.

The second type of databases is for plant phenotyping, where it is important to capture plant images without interfering the growth of plants. Thus, non-destructive imaging approaches are taken and the entire plant is imaged. The LSC database [Scharr et al., 2014] is the most relevant one to our database. It captures a large set of RGB images for the Arabidopsis and Tobacco plants. The provided manual labels allow the evaluation of leaf segmentation and leaf counting. In comparison, our MSU-PID database utilizes four sensing modalities in the data capturing, each providing different aspects of plant visual appearance. Our diverse manual labels also enable us to develop algorithms for additional applications such as leaf tracking and leaf alignment.

One of our data modalities is dense depth measurement. This has been a component of a number of recent non-plant RGB-D databases designed for object recognition [Lai et al., 2011], scene segmentation [Silberman & Fergus, 2011], human analysis [Sung et al., 2011,Barbosa et al., 2012], and mapping [Sturm et al., 2012]. By including dense depth for a plant database we anticipate enabling development of new 3D plant shape analysis algorithms.

3 Data Collection

3.1 Plants and Growth Conditions

Arabidopsis thaliana (ecotype Col-0) plants were grown at $20°C$, under a 16 hr:8 hr day night cycle with a daylight intensity set at 100 $\mu mol\ photons\ m^{-2}s^{-1}$. Black bean plants (*Phaseolus vulgaris L.*) of the cultivar Jaguar, were grown under a 14 hr:10 hr day night cycle with night and day temperatures of $18°C$ and $24°C$ respectively, and a daylight intensity set at 200 $\mu mol\ photons\ m^{-2}s^{-1}$. Note that the bean plants were watered with half-strength Hoaglands solution three times per week.

In all cases, seeds were planted in soil covered with a black foam mask in order to minimize the fluorescence background from algal growth. Two-week-old plants (*Arabidopsis* or bean) were transferred to imaging chambers and allowed to acclimate for 24 hours to the LED lighting before the start of the data collection. Growth conditions as described above were maintained for each set of plants for the duration of image collection.

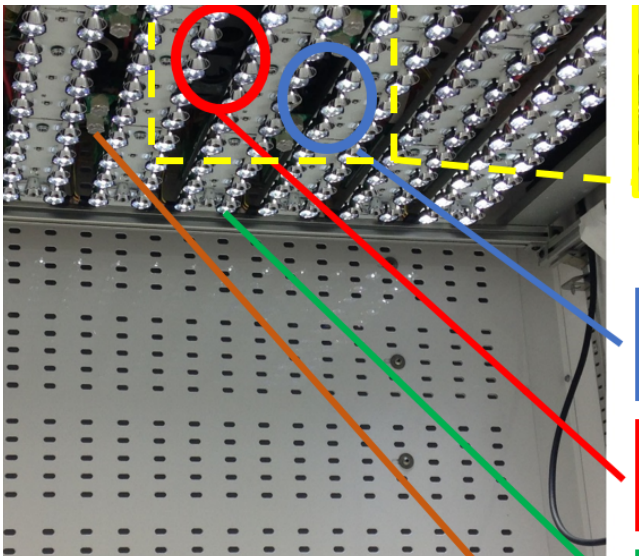

Fig. 2 The hardware setup for our data collection.

3.2 Hardware Setup

In this section, we introduce the hardware used for capturing fluorescence, IR, RGB color, and depth imagery data for both plants. Figure 2 illustrates the hardware and imaging setup used in our data collection.

3.2.1 Fluorescence and IR Images

Chlorophyll *a* fluorescence images were captured once every hour during the daylight period in a growth chamber [Cruz et al., 2015]. A set of 5 images were captured using a Hitachi KP-F145GV CCD camera (Hitachi Kokusai Electric America Inc., Woodbury, NY) outfitted with an infrared long pass filter (Schott Glass RG-9, Thorlabs, Newton, NJ), during a short period ($< 400\ ms$) of intense light saturating to photosynthesis ($> 10,000\ \mu mol\ photons\ m^{-2}s^{-1}$) provided by an array of white Cree LEDs (XMLAWT, 5700K color temperature, Digi-Key, Thief River Falls, MN) collimated using a 20 mm Carclo Lens (10003, LED Supply, Lakewood, CO). Chlorophyll *a* fluorescence was excited using monochromatic red LEDs (Everlight 625 nm, ELSH-F51R1-0LPNM-AR5R6, Digi-Key), collimated using a Ledil reflector optic ($C11347\_REGINA$, Mouser Electronics, Mansfield, TX) and pulsed for 50 μs during a brief window when the white LEDs were electronically

shuttered. In addition, a series of 5 images were also collected in the absence of the excitation light for artifact subtraction.

Infrared images were collected once every hour with the same camera and filter used for chlorophyll *a* fluorescence. Pulses of 940 *nm* light were provided by an array of OSRAM LEDs (SFH 4239, Digi-Key), collimated using a Polymer Optics lens (Part no. 170, Polymer Optics Ltd., Berkshire, England). Since 940 *nm* light does not influence plant development or drive photosynthesis, images were also collected during the night period [Eskins, 1992]. Precisely, phytochromes are the closest photoreceptors that absorb in the far red, near infrared region, but the action spectrum is diminished to zero or near zero (> 800 *nm*) in the region where we do IR reflectance (940 *nm*) [Butler et al., 1964]. Note that the other modalities were captured only at day time, so that they will not interfere plant growth.

Sets of 15 images were collected for averaging, in the absence of saturating illumination. As with chlorophyll *a* fluorescence, images were captured in the absence of 940 *nm* light for artifact subtraction.

3.2.2 RGB Color and Depth Images

The RGB color and depth images were collected using a Creative Senz3D sensor [Nguyen et al., 2015]. The sensor contains both a 1280×720 color camera directed parallel to, and separated by roughly 25 *mm* from, a depth camera which has a resolution of 320×240 pixels. The depth sensor uses a flash near IR illuminator and measures the time-of-flight [Hansard et al., 2013] of the beam at each pixel to obtain depth estimates along with an IR reflectance at each pixel.

There are a number of limitations to the depth sensor that become the sources of depth errors. The primary measurement limitation on the range-to-target is the strength of the reflected beam. As a result, dark, matt surfaces are measured reliably only at a close range on the order of 20 or 30 *cm*. Highly reflective surfaces also pose problems with direct reflections leading to saturation and highly unreliable depths. In addition reflective surfaces at grazing angles are less reliably measured since little signal is reflected. Fortunately the primary goal of the depth measurements are to obtain leaf depths, and plants provide good, roughly Lambertian, reflections of IR [Chelle, 2006]. Thus the depth pixels that are most reliable and are of most use are those that fall on plant foliage.

3.2.3 Image collection

The imagery data, including the fluorescent image, the IR reflectance image, the color image, and the 3D depth image, were collected once every hour. First, the fluorescent image and the IR reflectance image were captured sequentially using the same camera without any delay. After five minutes, the 3D depth image and the color image were captured using the Creative Senz3D sensor. The captured depth points were then transformed into the world coordinates and expressed in the unit of *mm*. Since plant leaves do not move quickly, the five minutes gap between the camera operations do not cause severe problems in image calibration.

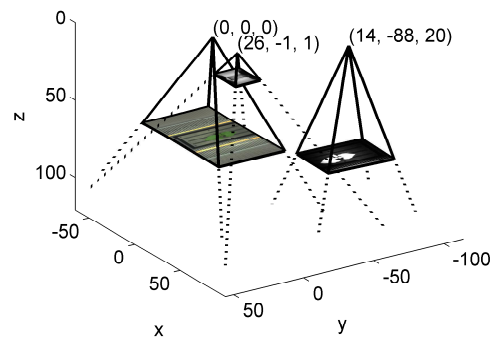

(*a*)

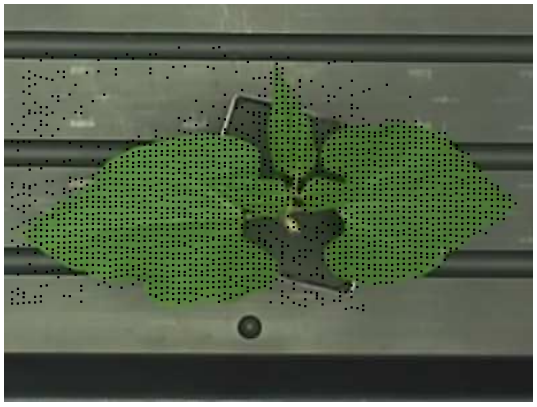

(*b*)

Fig. 3 (*a*)A plot of the three cameras showing their relative configuration and fields of view as obtained through calibration. Units are in *mm*, and distance to the target bean plant is roughly 620*mm* in this example. The image planes are plotted at depths proportional to the focal lengths. The optical center of the color camera (left-most) defines the world coordinate system. Close to it is the depth camera having much lower resolution. The right-most camera is the combined fluorescent and IR camera. (*b*) 3D points from the depth camera are projected along their rays into the world coordinates and then projected into the color and fluorescent camera images. This shows the projection into the color image (with 90° rotation for economical use of space). Only points in a rectangular region around the plant in the depth image are selected, and these are further filtered by eliminating points with high standard deviation. An algorithm requiring only 3D points on the plant could select only those that fall on the leaf pixels.

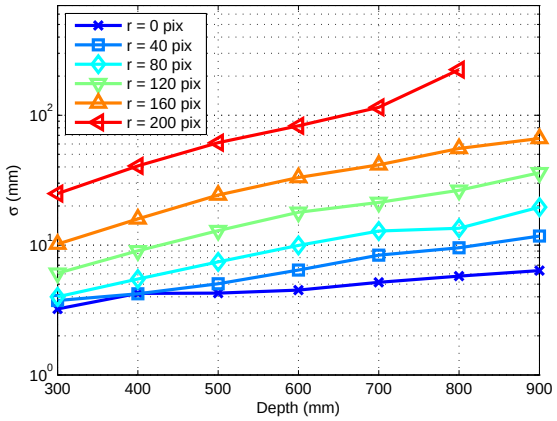

Fig. 4 Noise analysis for a depth camera obtained by imaging a flat surface at various depths. We found that the standard deviation, $\sigma_I(d,r)$ from Eq. (2) of the pixel depth measurements had a large dependency on both the target depth, d, and the pixel radius, r, from the image center, and these are plotted. A radius of 0 pixels is the image center, and of 200 pixels corresponds to the corners of the depth camera, which can be seen to have far larger standard deviation than at the image center for the same depth.

3.3 Sensor Calibration

A planar checkerboard pattern was used to calibrate all three cameras to obtain both intrinsic and extrinsic parameters. While the grid pattern is not visible in the depth image, it is nevertheless observed in the reflected IR image whose pixels correspond to the depth pixels. This enables the use of Zhang's method [Zhang, 2000] to calculate the intrinsic parameters including a 2-parameter radial distortion of each camera. In this process the poses of all three cameras are also calculated relative to the checkerboard. The intrinsic and extrinsic parameters are stored as text files, and a Matlab function is provided that reads the parameters and can plot the camera poses as in Figure 3.

3.3.1 Noise Characterization

The time of flight depth measurements can have significant noise, and it is useful to both model it and quantify it. Doing so can lead to strategies to reduce noise as well as providing guidance to algorithms that use the depth measurements. Our goal in this section is to provide a simple noise model that can predict the empirically observed depth noise on smooth, Lambertian surfaces, such as plant leafs.

The depth noise, ε, is modeled as the sum of an image dependent term, ε_I, and a sensor dependent term, ε_S:

$$\varepsilon = \varepsilon_I + \varepsilon_S. \tag{1}$$

The term ε_I is a random variable for each pixel with a value that varies between subsequent images taken from a fixed pose of a static scene. On the other hand, ε_S is a random variable for each pixel that models its depth offset, and its value only changes when the scene changes. The variance of ε_I is estimated for each pixel of a fixed scene observed over multiple images. In our experiments we observed a flat, uniform albedo surface perpendicular to the camera at a sequence of depths, and for each depth acquired 300 images. Object depth, d, has a large impact on ε_I. For constant depth, we observed that the primary factor affecting the variance is the pixel radius, r, from the image center. Physically we expect this dependence is due to a circularly symmetric illuminating beam closely aligned with the optical axis. Based on these observations we model $\sigma_I(d,r)$, the standard deviation of ε_I, as a function of depth and pixel radius. From our experiments we build up a lookup table for this as plotted in Figure 4.

Averaging over repeated images of a scene will not remove all the depth error as there are pixel depth offsets that are constant for images of the same scene. We model these with ε_S. To estimate its standard deviation, σ_S, we first average over many depth measurement images, in our case 300, to obtain pixel depth estimates that approximately eliminate the effect of ε_I. Then by calculating true ray depths on a known surface, in our case the observed plane, and further assuming that ε_S has the same standard deviation for all pixels, σ_S is obtained as the standard deviation of the error between averaged depths and known depths. In our experiments we obtained $\sigma_S = 6.5mm$, and found that it was insensitive to changes in depth.

The recorded depth images in the data collection are the result of averaging $N = 5$ subsequent depth images. Assuming independence of ε_I and ε_S, the variance of pixel depth measurements is given by:

$$\sigma^2(d,r) = \frac{\sigma_I^2(d,r)}{N} + \sigma_S^2. \tag{2}$$

There are additional sources of noise not modeled by this. Object albedo has an impact although this is fairly weak for strong signal reflections. Factors with large impact on signal noise include: object specularities, sharp variations in object albedo, mixed-depth pixels on object edges, and cases of very-low signal reflection, all of which can lead to very large variances. One of the utilities of having a model for variance is that it can be compared with the measured variance, and the difference used as a cue for portions of the scene that violate our modeling assumptions.

In addition, we noticed that the chamber light shades blocked some of the depth camera field of view, and in doing so reflected some of the IR illumination.

Table 2 Summary of Arabidopsis and Bean databases.

Plants	Subjects	Days	Images/Day	Total Images	Annotated Images
Arabidopsis	16	9	16	2304×4	576×4
Bean	5	5	14	350×4	175×4

Table 3 Plant image resolution of Arabidopsis and Bean databases, computed based on the yellow ROIs in Figure 1.

Plants	fluorescence	IR	RGB	depth
Arabidopsis	$\sim 240 \times 240$	$\sim 240 \times 240$	$\sim 120 \times 120$	$\sim 25 \times 25$
Bean	1000×640	1000×640	380×720	90×190

This resulted in a small constant depth shift for the pixels. We measured this shift for each chamber experiment and provide it as an optional correction to the depth images.

4 Annotation, Files and Protocol

4.1 Data Statistics

MSU-PID includes two subsets, one for each plant type: Arabidopsis and Bean. The statistic information of these two subsets are summarized in Table 2. The images were acquired every hour. As there is no light at night hours, plants can not be imaged by the fluorescence and RGB color sensors while IR and depth cameras can still perform the capturing in the night. In order to make sure that all four modalities are present at each imaging opportunity, we release the part of images captured only in the day time, which are 16 images per day for Arabidopsis and 14 for bean for all four modalities.

The two subsets differ in plant image resolutions. As shown in Figure 1, we grow and image a single bean plant while a whole tray of Arabidopsis are grown at the same time. Therefore, the resolution of a Arabidopsis plant is much lower than that of a bean plant. We manually crop 16 Arabidopsis plants, which have been captured by all four sensors simultaneously. Table 3 summaries the image resolution of each plant in all four modalities.

4.2 Manual Annotations

Part of the database is manually annotated to provide ground truth tip locations, leaf segmentation results and leaf consistency overtime. Tip locations are saved in a TXT file for each frame. Leaf segmentation results are stored in a PNG image for each frame with one color for each leaf. The same color is used to represent the same leaf over a sequence of frames.

We use the fluorescence images as the input for labeling because of their simple and uniform background. For Arabidopsis images, we label 4 frames each day. While for bean images, we label 7 frames each day because of their spontaneous and faster leaf movement. A Matlab-based GUI interface is developed for leaf labeling, as shown in Figure 5, which will also be available to the public. A user can open a plant image to label the two tips and annotate each leaf segment. The results will be automatically saved once a user moves onto the next image for labeling. For consistent annotation of the same leaf over time, we show a number on the center of each leaf indicating the order of labeling from the previous frame.

The labeling of leaf tips is implemented by clicking pairs of points on the image. The outer tip is always clicked first before the inner tip. For visualization, a line connecting each pair of tips will be shown immediately after clicking the inner tip. Inaccurate labels can be deleted by clicking the right button of the mouse near the labeled point and relabeled by clicking the left button again.

The labeling of the leaf segment is implemented by clicking the boundary of one leaf at each time. In order to provide more accuracy labeling, we click very dense points ($\sim$ 20 points on average) on the boundary. The labeled leaf boundary is overlaid on the image for better visualization to guide the next action. Incorrect label can be deleted right after the labeling. This process continues until all leaf segments have been annotated. After the labeling of one plant, we visually go through the results and correct inaccurate labels. One example of the labeling results for one plant is shown in Figure 8 (b), where one color is used to represent each specific leaf. As we can see during the transition between day 5 and day 6, there is one leaf showing up and covering up the leaf underneath, which disappears and will not be annotated later. In total, we labeled 5142 leaves.

Note that one alternative approach for labeling leaf segments is to directly label the membership of superpixels instead of drawing a polygon along the boundary.

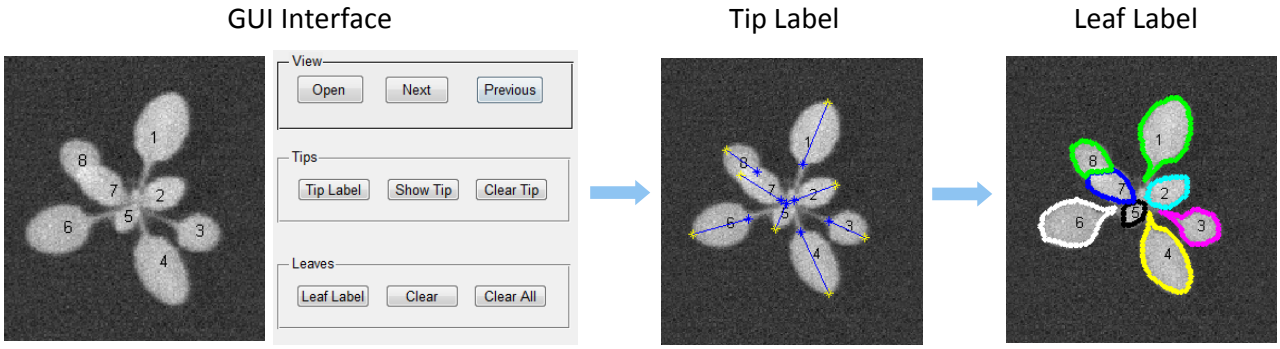

Fig. 5 Leaf labeling process, including tip labels and leaf segmentation annotation.

Our experience is that since a noticeable percentage of extracted superpixels cover pixels of two neighboring leaves, the extra effort of breaking a super pixel into two makes it a less efficient alternative.

4.3 Name Conventions and File Types

We release training and testing sets in two separate folders. In each folder, there are two subfolders named Arabidopsis and Bean. The files in each subfolder have the following form:

- plant_ID_day_X_hour_YY_rgb.png: the original RGB color images;
- plant_ID_day_X_hour_YY_fmp.png: the original fluorescence images;
- plant_ID_day_X_hour_YY_ir.png: the original IR images;
- plant_ID_day_X_hour_YY_depth.png: the original depth images;
- plant_ID_day_X_hour_YY_depthSigma.png: the depth standard deviation images;
- plant_ID_day_X_hour_YY_label.png: the labeled images of fluorescence modality;
- plant_ID_day_X_hour_YY_tips.txt: the labeled tip locations;

where ID indicates the plant subject ID number (1 to 16 for Arabidopsis, 1 to 5 for bean), X is an integer indicating the date ($1-9$ for Arabidopsis, 1 to 5 for bean), and YY represents the image index within a day ($1-16$ for Arabidopsis, 1 to 14 for bean). For each combination of day and hour, we provide four modalities in PNG files (_rgb, _fmp, _ir, _depth). For annotated images, we have two additional files (_label, _tips) saving the annotation results. Leaf segmentation results are encoded as indexed PNG files, where each leaf is assigned a unique and consistent leaf ID over time. Leaf ID starts from 1 and continuously increase till the total number of leaves. And the background is encoded as 0.

Tips locations are saved in TXT files where each line has the following format:

– leaf ID tip1_x tip1_y tip2_x tip2_y

where leaf ID is an integer number that is consistent with the segmentation label in the PNG file. tip1_x and tip1_y represent the coordinates of the outer tip point. tip2_x and tip2_y represent the coordinates of the inner tip point.

In addition to the original images and annotation results, we provide another folder named Matlab with all Matlab functions that will be used for mapping between different image modalities and for the purpose of performance evaluation. Note that the annotation is provided based on fluorescence images. In order to evaluate methods developed on other modalities, we provide image-mapping functions between every two modalities. The total storage of our database is around $380MB$, which is convenient for downloading via Internet.

4.4 Experimental Protocols

As shown in Table 1, MSU-PID can be used for applications such as leaf segmentation, leaf alignment, leaf tracking, and leaf counting. To facilitate future research, we separate the database into the training set and the testing set. 40% of the data is used for training and 60% for testing. Specifically, 6 plants of Arabidopsis and 2 plants of bean are selected for training. For fair comparison, both supervised learning and unsupervised learning methods should evaluate their performance on the training and testing sets separately. The user may decide to utilize one or multiple modalities of the plant imagery for training and testing respectively. The availability of multiple modalities allows user to design novel experimental setup. For example, using RGB and depth modalities for training and RGB for testing can take advantage of additional information during the learning

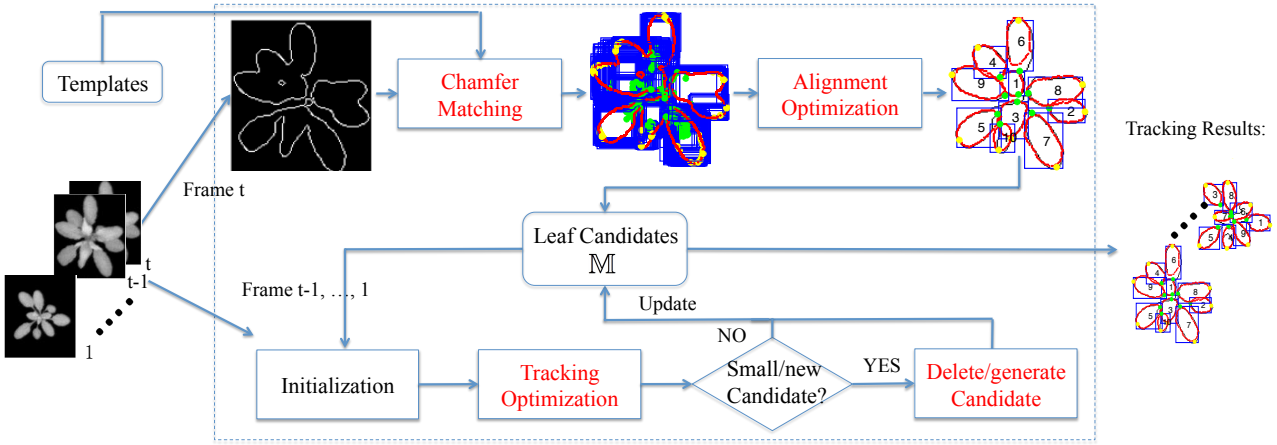

Fig. 6 Overview of the baseline method.

without incurring extra sensor cost during the testing, which can be implemented via either learning with side information [Chen et al., 2013], or transfering learning with missing modality [Ding et al., 2014].

Performance metric To evaluate the performance of leaf segmentation, alignment, and tracking, we use four performance metrics, whose Matlab implementations will be provided along with the data. Three of them are based on the tip-based error, which is defined as the average distance of a pair of estimated leaf tips $\hat{\boldsymbol{t}}_{1,2}$ with a pair of labeled leaf tips $\boldsymbol{t}_{1,2}$ normalized by the labeled leaf length:

$$e_{la}(\hat{\boldsymbol{t}}_{1,2}, \boldsymbol{t}_{1,2}) = \frac{||\hat{\boldsymbol{t}}_1 - \boldsymbol{t}_1||_2 + ||\hat{\boldsymbol{t}}_2 - \boldsymbol{t}_2||_2}{2||\boldsymbol{t}_1 - \boldsymbol{t}_2||_2}. \quad (3)$$

We build the frame-to-frame and video-to-video correspondence respectively and generate two sets of tip-based errors. More details can be find in [Yin et al., 2015]. We define a threshold τ to operate on the corresponding tip-based errors. By varying τ, we compute the first three metrics as follows:

- *Unmatched Leaf Rate (ULR)*, the percentage of unmatched leaves with respect to the total number of labeled leaves. This can attribute to two sources. The first is miss detections and false alarms. The second is matched leaves with tip-based errors larger than τ.
- *Landmark Error (LE)*, the average tip-based errors smaller than τ of all frame-to-frame correspondent leaves.
- *Tracking Consistency (TC)*, the percentage of video-to-video correspondent leaves whose tip-based errors are smaller than τ.

In order to evaluate the leaf segmentation accuracy, we adopt an additional metric [Scharr et al., 2014] based on the Dice score of estimated segmentation results and ground truth labels:

- *Symmetric Best Dice (SBD)*, the symmetric best Dice among all labeled leaves.

The Matlab function for computing *SBD* is provided by [Scharr et al., 2014]. The instructions on how to use the evaluation functions are included as comments of the function.

5 Baseline Method and Performance

To facilitate future research on this database, we provide a baseline approach and its performance by using the fluorescence modality of Arabidopsis.

5.1 Multi-leaf Segmentation and Tracking Framework

We apply our automatic multi-leaf segmentation and tracking framework [Yin et al., 2014a, Yin et al., 2014b] to the testing set of Arabidopsis fluorescence imagery to provide a baseline. Note that [Yin et al., 2014a, Yin et al., 2014b] is designed for rosette plants like Arabidopsis. Therefore, it will not be applied to bean plant as it does not belong to rosette plants. We treat all images in 9 days as a video from first image on the first day to the last image in the last day. As shown in Figure 6, the input of this framework is a plant video and a set of predefined templates with various shapes, scales, and orientations. To generate the template set, we first select 12 templates with different aspect ratios from the labeled images in the training set together with the corresponding tip locations. For each template, we scale it to 10 different sizes in order to cover the

entire range of leaf sizes in the database. For each scale template, we rotate every 15° to generate 24 templates at different orientations. Tip locations will be scaled and rotated accordingly. Finally, we generate 2,880 leaf templates.

Our work is motivated by Chamfer Matching technique [Barrow et al., 1977], which is used to align two edge maps. We extend it to simultaneously align multiple overlapping objects. For plant segmentation, we use simple thresholding and edge detection to generate an edge map and mask. The best threshold is learnt from the training set, which is done by tuning the threshold in a certain range and find the best one by evaluating the overlap of the segmented masks with the groundtruth label masks. The edge map and mask are used in the alignment and tracking optimization.

First, we find the best location of each template in the edge map that has the minimal Chamfer matching distance, which will result in an over-completed set of leaf candidates. Second, we apply multi-leaf alignment [Yin et al., 2014a] approach to find an optimal set of leaf candidates on the last frame of the video, which will provide the information of the number of leaves, tip locations and boundaries of each leaf. Third, we apply multi-leaf tracking [Yin et al., 2014b] approach, which is based on leaf template transformation, to track leaves between continuous two frames.

In the tracking process, we delete a leaf when it becomes too small. We develop a procedure to generate new leaves when there is a relatively large portion of the mask has not been covered by current leaf candidates. For each frame of the video, we can generate a label image with each leaf being labeled with one color and the tip locations for each estimated leaf. The labeled color for each leaf in the video remains the same during the tracking process.

5.2 Performance and Analysis

We apply our algorithm to all 144 frames of each video and evaluate the performance on labeled 36 frames. Leaf alignment is applied to the last frame of each video. Figure 7 shows some examples of leaf alignment results. Our framework works very well on segmenting large leaves with no overlap to neighbor leaves. For overlapping leaves, it becomes more challenging as the edges in the overlapping area are more difficult to be detected. However, when the overlapping leaves are further away from the center, they will have a higher chance to be detected as shown in (c) of Figure 7. When the overlapping leaves are close to the center, smaller leaves will be covered by larger leaves as shown in $(a), (d), (e)$ of Figure 7.

Leaf alignment provides the leaf candidates for tracking over time. Figure 8 shows the leaf tracking result of one video. The leaf template transformation works well for most of the leaves. As plant grows, younger leaves may grow faster than older leaves and occlude the older leaves. As shown in Figure 8 (b), purple leaf replaces the red leaf at day 6. Our backward tracking algorithm tracks leaves from the last frame to the first frame. The two leaves are still being considered as one leaf (ID 8) in day 4 and day 3. Leaf 8 in day 1 and 2 is a leaf ID switch w.r.t. the purple ground truth leaf and will not be considered as a consistently tracked leaf. However, they are still evaluated as well aligned and segmented leaves.

For quantitative evaluation, we vary τ from 0 to 1 and generate the first three evaluation metrics, as shown in Figure 9. *ULR* decreases as τ increases as more leaves are being considered as matched leaves. As τ keeps increasing, *ULR* approaches a constant value, which is the different number in leaf counting that results from both miss detection and false alarms. *LE* increases as τ increases as it includes leaves with larger tip-based errors for averaging. *TC* increases as τ increases as more leaves are being considered as correctly tracked leaves. Note that *TC* is influenced by the length of frames evaluated for each video. As the longer frames we evaluate, the higher chance tracking will fail. Overall, our method can detect 87% and track 50% of all labeled leaves with less than 20% average tip-based errors.

We generate a label image for each frame based on the leaf segmentation results and compute the *SBD* score for each labeled image. The average *SBD* over all images is 0.61.

6 Conclusions

This paper presents a newly collected multi-modality plant imagery database, "MSU-PID". Compared to existing databases in the field, MSU-PID not only has multiple calibrated modalities, but also enables a wide variety of plant image analysis applications. Therefore, we believe this new database will be beneficial to the research community in terms of algorithm development, performance evaluation, and identifying new research problems in plant image analysis. Furthermore, we are also open to suggestions and comments from the users of this database to further enhance our imaging setup and capturing protocol, so that we can develop new databases in the future.

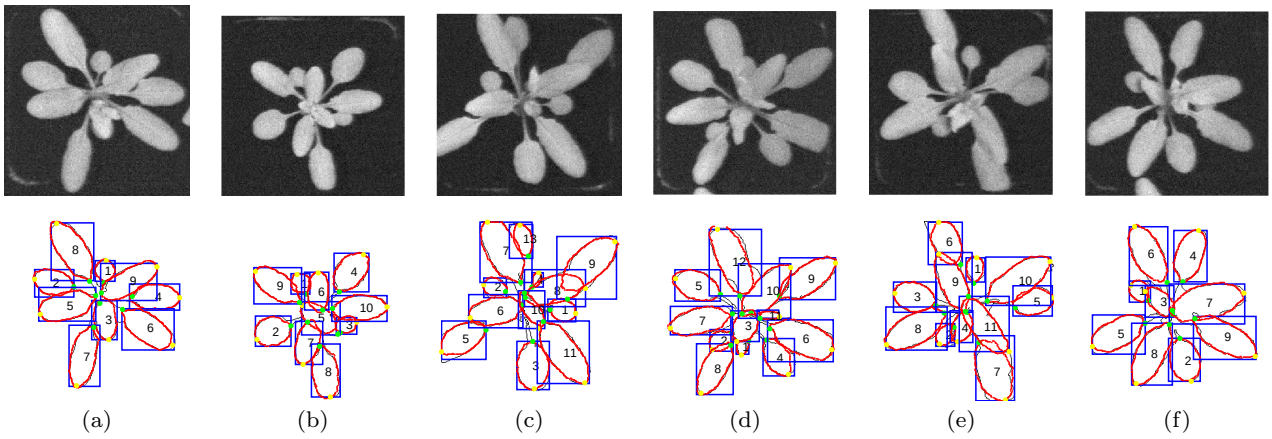

Fig. 7 Leaf alignment results on the last frame of 6 plant videos. First row shows the original images. Second row shows the alignment results with red points denoting the boundary of the leaf templates in the blue bounding boxes. The numbers on the leaves are the leaf IDs representing the order of the leaf being selected and they will be consistent during tracking.

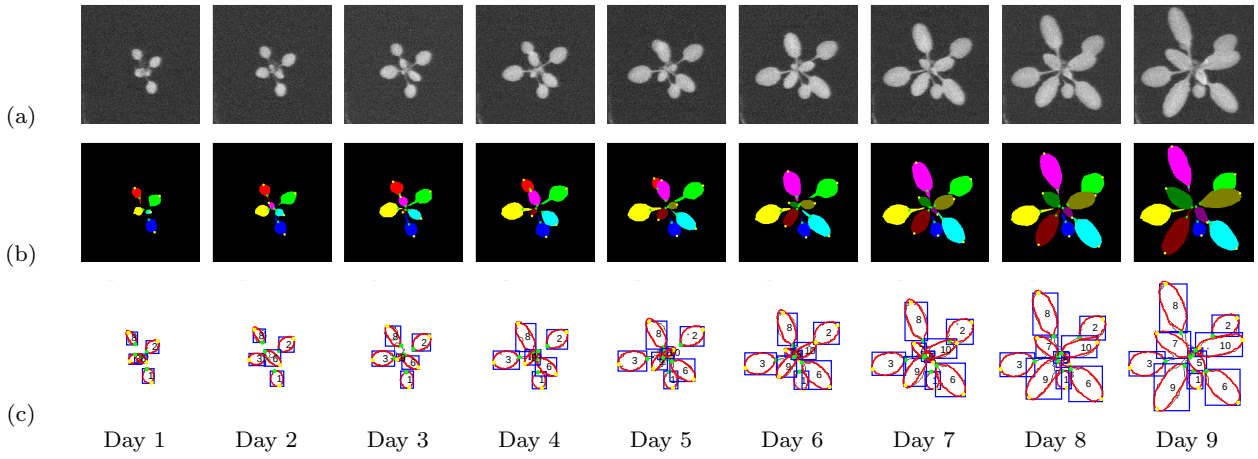

Fig. 8 Tracking result for one video with one frame for each day. (*a*) Example frames in the video. (*b*) Leaf label results overlaid with tip locations. (*c*) Leaf tracking results.

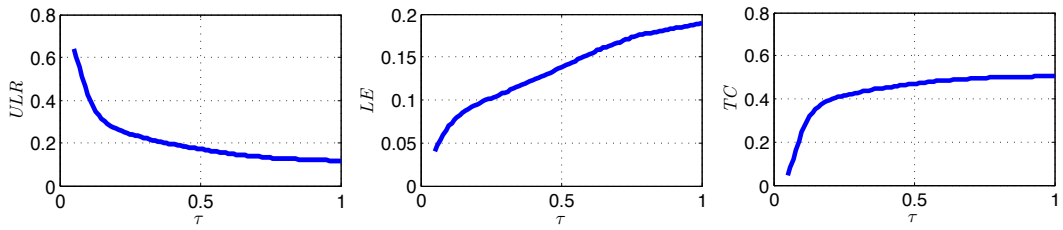

Fig. 9 Performance of the baseline method on the testing set of the fluorescence modality of Arabidopsis plant.

References

[Barbosa et al., 2012] Barbosa, Igor Barros, Marco Cristani, Alessio Del Bue, Loris Bazzani, & Vittorio Murino 2012. Re-identification with rgb-d sensors. In First International Workshop on Re-Identification, pages 433–442.

[Barrow et al., 1977] Barrow, Harry G., Jay M. Tenenbaum, Robert C. Bolles, & Helen C. Wolf 1977. Parametric correspondence and Chamfer matching: Two new techniques for image matching. Technical report, DTIC Document.

[Butler et al., 1964] Butler, WL, SB Hendricks, & H-W Siegelman 1964. ACTTON SPECTRA OF PHYTOCHROME IN VITRO*. Photochemistry and Photobiology, 3(4):521–528.

[Chelle, 2006] Chelle, Michael 2006. Could plant leaves be treated as Lambertian surfaces in dense crop canopies to estimate light absorption? Ecological Modelling, 198(1):219 – 228.

[Chen et al., 2013] Chen, Jixu, Xiaoming Liu, & Siwei Lyu 2013. Boosting with side information. In Proc. Asian Conf. Computer Vision (ACCV), pages 563–577. Springer.

[Cruz et al., 2015] Cruz, JA, LJ Savage, R Zegarac, W Kovac, C Hall, J Chen, & DM Kramer 2015. Dynamic Environmental Photosynthetic Imaging (DEPI) Reveals Emer-

gent Phenotypes Related to the Environmental Responses of Photosynthesis. Nature Biotechnology, in revision.

[Ding et al., 2014] Ding, Zhengming, Shao Ming, & Yun Fu 2014. Latent low-rank transfer subspace learning for missing modality recognition. In Proc. of the AAAI Conference on Artificial Intelligence (AAAI).

[Döös, 2002] Döös, Bo R 2002. Population growth and loss of arable land. Global Environmental Change, 12(4):303–311.

[Erblichkeit, 1903] Erblichkeit, Johannsen W. 1903. Populationen und reinen Linien. Gustav Fischer Verlag.

[Eskins, 1992] Eskins, Kenneth 1992. Light-quality effects on Arabidopsis development. Red, blue and far-red regulation of flowering and morphology. Physiologia Plantarum, 86(3):439–444.

[Fahlgren et al., 2015] Fahlgren, Noah, Malia A Gehan, & Ivan Baxter 2015. Lights, camera, action: high-throughput plant phenotyping is ready for a close-up. Current opinion in plant biology, 24:93–99.

[Furbank & Tester, 2011] Furbank, Robert T, & Mark Tester 2011. Phenomics–technologies to relieve the phenotyping bottleneck. Trends in plant science, 16(12):635–644.

[Hansard et al., 2013] Hansard, Miles, Seungkyu Lee, Ouk Choi, & Radu Horaud 2013. Time-of-Flight Cameras: Principles, Methods and Applications. Springer, New York, NY.

[Haug & Ostermann, 2014] Haug, Sebastian, & Jörn Ostermann 2014. A Crop/Weed Field Image Dataset for the Evaluation of Computer Vision Based Precision Agriculture Tasks. In Proc. European Conf. Computer Vision Workshops (ECCVW), pages 105–116. Springer.

[Houle et al., 2010] Houle, D, DR Govindaraju, & S Omholt 2010. Phenomics: the next challenge. Nature Review Genetics, 11(12):855–866.

[Huang et al., 2007] Huang, Gary B., Manu Ramesh, Tamara Berg, & Erik Learned-Miller 2007. Labeled Faces in the Wild: A Database for Studying Face Recognition in Unconstrained Environments. Technical Report 07-49, University of Massachusetts, Amherst.

[Kumar et al., 2012] Kumar, Neeraj, Peter N. Belhumeur, Arijit Biswas, David W. Jacobs, W. John Kress, Ida C. Lopez, & João VB. Soares 2012. Leafsnap: A computer vision system for automatic plant species identification. In Proc. European Conf. Computer Vision (ECCV), pages 502–516. Springer.

[Lai et al., 2011] Lai, Kevin, Liefeng Bo, Xiaofeng Ren, & Dieter Fox 2011. A large-scale hierarchical multi-view rgb-d object dataset. In IEEE International Conference on Robotics and Automation (ICRA), pages 1817–1824.

[Minervini et al., 2015] Minervini, Massimo, Hanno Scharr, & Sotirios A. Tsaftaris 2015. Image analysis: the new bottleneck in plant phenotyping. To appear in: IEEE Signal Processing Magazine.

[Nguyen et al., 2015] Nguyen, VD, MT Chew, & S Demidenko 2015. Vietnamese sign language reader using Intel Creative Senz3D. In IEEE International Conference on Automation, Robotics and Applications (ICARA), pages 77–82.

[Phillips et al., 2000] Phillips, P. J., H. Moon, P. J. Rauss, & S. Rizvi 2000. The FERET evaluation methodology for face recognition algorithms. IEEE Trans. Pattern Anal. Mach. Intell., 22(10):1090–1104.

[Scharr et al., 2014] Scharr, Hanno, Massimo Minervini, Andreas Fischbach, & Sotirios A Tsaftaris 2014. Annotated image datasets of rosette plants. Technical Report FZJ-2014-03837.

[Silberman & Fergus, 2011] Silberman, Nathan, & Rob Fergus 2011. Indoor scene segmentation using a structured light sensor. In IEEE International Conference on Computer Vision Workshops (ICCV Workshops), pages 601–608.

[Söderkvist, 2001] Söderkvist, Oskar 2001. Computer vision classification of leaves from swedish trees. Master thesis, Linköping University.

[Sturm et al., 2012] Sturm, Jürgen, Nikolas Engelhard, Felix Endres, Wolfram Burgard, & Daniel Cremers 2012. A Benchmark for the Evaluation of RGB-D SLAM Systems. In Proceedings of the International Conference on Intelligent Robot Systems (IROS), pages 573–580.

[Sung et al., 2011] Sung, Jaeyong, Colin Ponce, Bart Selman, & Ashutosh Saxena 2011. Human Activity Detection from RGBD Images. CoRR, 64.

[Walter et al., 2015] Walter, Achim, Frank Liebisch, & Andreas Hund 2015. Plant phenotyping: from bean weighing to image analysis. Plant methods, 11(1):14.

[Wu et al., 2007] Wu, Stephen Gang, Forrest Sheng Bao, Eric You Xu, Yu-Xuan Wang, Yi-Fan Chang, & Qiao-Liang Xiang 2007. A leaf recognition algorithm for plant classification using probabilistic neural network. In IEEE International Symposium on Signal Processing and Information Technology, pages 11–16.

[Yin et al., 2014a] Yin, Xi, Xiaoming Liu, Jin Chen, & David M Kramer 2014a. Multi-Leaf Alignment from Fluorescence Plant Images. In IEEE Winter Conf. on Applications of Computer Vision (WACV), Steamboat Springs CO.

[Yin et al., 2014b] Yin, Xi, Xiaoming Liu, Jin Chen, & David M Kramer 2014b. Multi-Leaf Tracking from Fluorescence Plant Videos. In Proc. Int. Conf. Image Processing (ICIP), Paris, France.

[Yin et al., 2015] Yin, Xi, Xiaoming Liu, Jin Chen, & David M Kramer 2015. Joint Multi-Leaf tracking from Fluorescence Plant Videos. arXiv preprint arXiv:submit/1245553.

[Zhang, 2000] Zhang, Zhengyou 2000. A flexible new technique for camera calibration. Pattern Analysis and Machine Intelligence, IEEE Transactions on, 22(11):1330–1334.